Determination of the Charge Transport Mechanisms in Ultra-Thin Copper Phthalocyanine Vertical Heterojunctions

Carlos C. Bof Bufon[†, §,], Céline Vervacke[†], Dominic J. Thurmer[†], Michael Fronk[‡], Georgeta Salvan[‡], Susi Lindner[∥], Martin Knupfer[∥], Dietrich R. T. Zahn[‡] and Oliver G. Schmidt[†, ⊥]*

[†]Institute for Integrative Nanosciences, IFW Dresden, Helmholtzstrasse 20, 01069 Dresden, Germany.

[⊥]Material Systems for Nanoelectronics, Chemnitz University of Technology, Reichenhainerstrasse 70, 09107 Chemnitz, Germany.

[‡]Semiconductor Physics, Chemnitz University of Technology, Reichenhainerstrasse 70, 09107 Chemnitz, Germany

[∥]Institute for Solid State Research, IFW Dresden, Helmholtzstrasse 20, 01069 Dresden, Germany.

[§]Brazilian Nanotechnology National Laboratory, CNPEM, PO Box 619, 13083-970, Campinas, Brazil

Supporting information

1) Fabrication of the heterojunction

The Au/CuPc/Au heterojunctions were fabricated on Si (100) wafers covered by 1 µm SiO_2. The first fabrication step is the creation of the finger-like (mesa) structure by patterning and etching 270 nm of the SiO_2 layer in buffered HF solution (6.5:34.8 %w/w HF:NH_4F) for a few seconds (Figure S1a). Afterwards the mesa is covered by a Cr/Au (5/20 nm) conducting layer (Figure S1b) by thermal evaporation. In all steps, the patterning is done by conventional photolithography. Next in the sequence, as illustrated in Figure S1c, a contact pad is patterned overlapping the finger-like structure by depositing Cr/Au (5/50 nm) again. Before depositing the strained layer, a Ge layer (20 nm) is patterned (Figure S1d) and further oxidized into GeO_x.

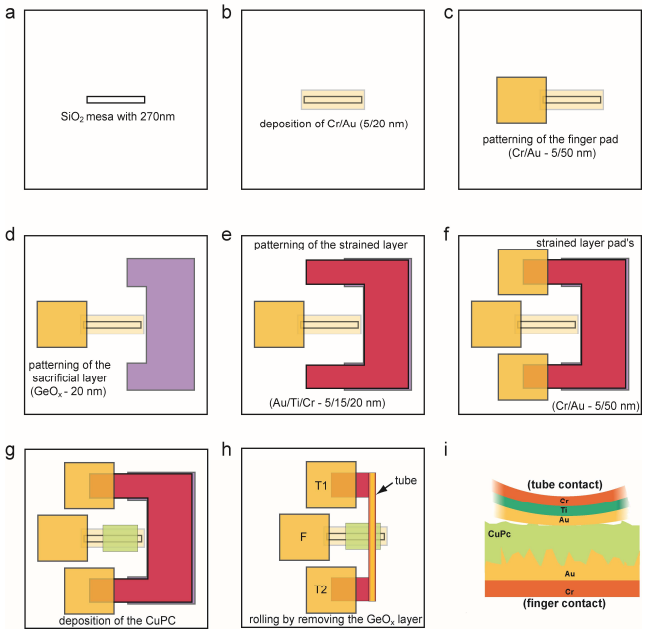

Figure. S1. (a-h) Fabrication scheme of the Au/CuPc/Au heterojunction. (i) Au/CuPc/Au interfaces (not on scale).

The fabrication process used for preparing the sacrificial layer is described in detail elsewhere[1,2]. Next, the strained layer, consisting of a tri-metallic Au/Ti/Cr nanomembrane (5/15/20 nm), is deposited by electron-beam evaporation on top of the GeO_x sacrificial layer (Figure S1e). Here, the Ti/Cr bimetallic layer creates the strain gradient necessary

for tube formation, while the bottom Au layer is used as the contact layer for the CuPc after rolling. Lastly, the pads for the strained layer (later the tube structure) are fabricated (Figure S1f).

Preceding the rolling process, a thin film of CuPc (6-10 nm) is deposited through a photo-resist mask (Figure S1g). The deposition was done using organic molecular beam deposition (OMBD) in vacuum with a base pressure of 10^{-7} mbar. The sample was exposed to the molecular beam for 20 minutes at a constant rate of 0.5 nm/min. During the process the sample was not cooled or heated. After the CuPc deposition, the lift-off was performed in acetone. No signature of degradation was detected in the CuPc thin film after the lift-off procedure. Next, the rolling is performed, facilitated by the self-release of the strained metallic nanomembrane through selective removal of the GeO_x sacrificial layer in pure deionised H_2O. The contact between the tube and finger is formed after 2 hours of rolling. Alternatively, the required rolling time can be controlled by changing the GeO_x composition and etching solution.[2]

After the rolling process, the tube-like electrode rests on top of the metallic finger establishing an electrical connection to the CuPc layer (Figure S1g). Notice that the contact to the tube electrode is established by the Au layer, which is the outermost layer of the tube (Figure S1i). Finally, after completion the samples are placed in a vacuum chamber for 24 hours.

2) Scanning electron microscopy (SEM)

The as-processed devices were imaged using a Zeiss Cross-beam® with 5-30 kV acceleration voltage. Images were typically obtained using 5 kV to reduce damage to the sample from the electron beam. The cross-sectional images were obtained using an attached Ga-ion focused ion beam (FIB) milling column for vertical cutting, followed by

SE imaging. A scanning electron microscopy (SEM) image of a device array and the SEM cross section of the heterojunction are highlighted in Figure S2a, respectively.

3) Surface analysis of CuPc thin films

All the AFM measurements were performed using an AFM DI3100 from Veeco while the analysis was done with the software Nanoscope.

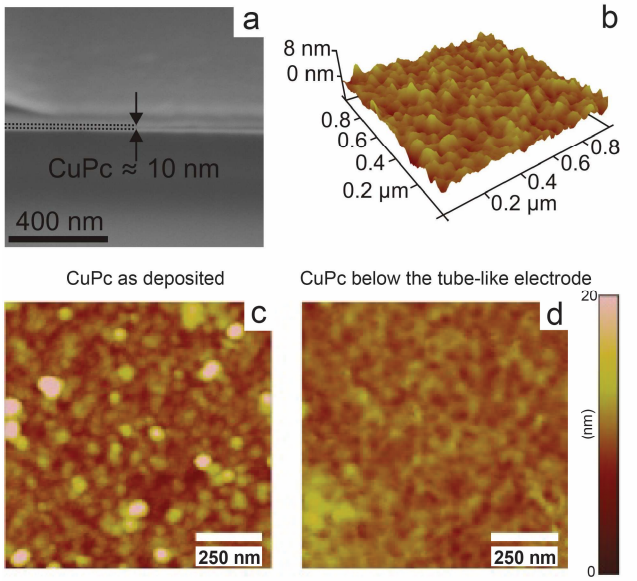

Figure S2. (a) SEM cross section of the Au/CuPc/Au interfaces. (b) AFM image of the CuPc film below the contacting tube. (c) AFM image of a CuPc film surface as deposited and (d) after the removal of the tube tube from its surface.

For comparison, Figure S2c shows the AFM image of a CuPc film as-deposited and after the removal of the tube from its surface (Figure S2d). It is clear that the tube flattens the CuPc surface. We observe that the external side of the tube has the same roughness of the sacrificial layer, which is smaller than 1 nm. This roughness is also transferred to the CuPc by rolling the tube on it. Therefore, besides of forming an effective electrical contact, the rolled-up nanomembrane works as a micro-roller to flatten (maybe even compact them) soft and rough films.

The geometric contacting area at the tube-finger junction was estimated taking the foot print left by the tube electrode on top of the organic layer into account (see Figure S3a).

In average, the value obtained is 3.0±1.5 μm^2. The current density as a function of the electric-field is shown in Figure S3b.

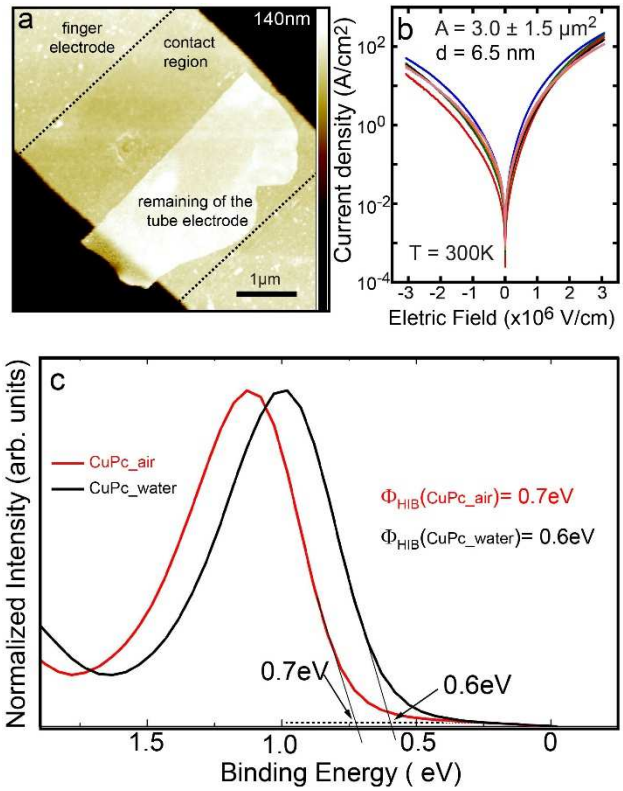

Figure S3. (a) AFM image of the finger-like electrode after removal of the tube-shaped nanomembrane from the top of the CuPc layer. The region between the dashed lines is the geometric contacting area. (b) Current density as a function of the electric field. (c) Valence band photoemission spectra of the two different CuPc samples (air and water exposed) taken with a photon energy of 21.21 eV up to 1.9 eV BE. Note: The dashed lines show the determination of the hole injection barrier Φ_{HIB}.

For the photoelectron measurements shown in Figure S3c, CuPc films with a nominal thickness of 10 nm were deposited on top of Cr/Au (5/20 nm) evaporated electrodes. The substrate was a <100> silicon wafer covered by 1 μm SiO_2. In order to reproduce the effects of the rolling solution, one sample was immersed in deionized water for 150 minutes before measurement whereas a second one was measured as-deposited. The ultra-violet photoelectron spectroscopy (UPS) experiments were carried out using a commercial PHI 5600 spectrometer. Photons with energy of 21.21 eV from a He discharge lamp were used to perform valence band measurements. The UPS

measurements were done by applying a sample bias of -5 eV to obtain the correct sample determined secondary electron cut-off. The total energy resolution of the spectrometer, determined by analyzing the width of the Au Fermi edge, was about 0.1 eV.

4) Low temperature measurements.

The low temperature measurements were performed in a Lakeshore helium flow cryogenic probe station in ultra-high vacuum (10^{-7}mTorr). The temperature measurements were done below the samples. In order to guarantee the temperature stability the temperature was also monitored in one of the probe arms. The samples were fixed to the cryostat cold finger by using silver paint. Temperature calibrations were done previously in this system by monitoring superconducting transitions on Nb samples.[3] The I-V characteristics were obtained by using a Keithley model 2636source-meter.

5) Fowler-Nordheim plot.

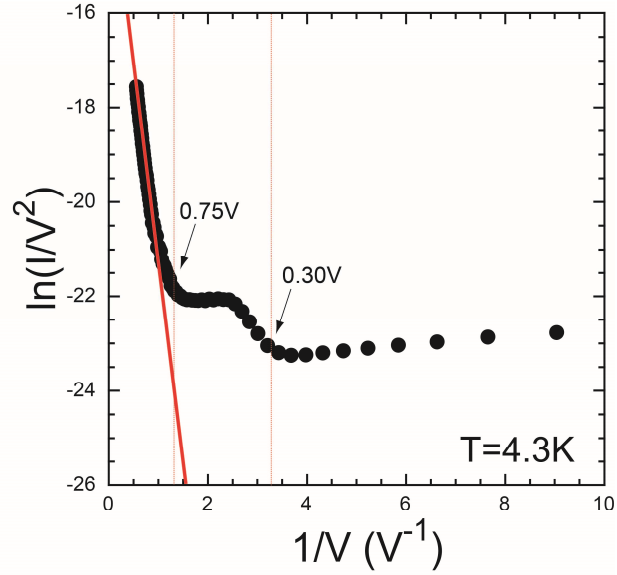

Figure S4. Fowler-Nordheim plot for the Au/CuPc/Au heterojunction, measured at 4.3 K. For V < 0.26 V, the transport takes place by the direct tunneling across the CuPc barrier. For V > 0.75 V, a transition to Fowler-Nordheim tunneling takes place. The red line indicates the best linear fit.

6) References

(1) Bof Bufon, C. C.; Arias Espinoza, J. D.; Thurmer, D. J.; Bauer, M.; Deneke, C.; Zschieschang, U.; Klauk, H.; Schmidt, O. G. Hybrid Organic/Inorganic Molecular

Heterojunctions Based on Strained Nanomembranes. *Nano Lett* **2011**, *11*, 3727–3733.
(2) Bof Bufon, C. C.; Cojal González, J. D.; Thurmer, D. J.; Grimm, D.; Bauer, M.; Schmidt, O. G. Self-Assembled Ultra-Compact Energy Storage Elements Based on Hybrid Nanomembranes. *Nano Lett* **2010**, *10*, 2506–2510.
(3) Thurmer, D. J.; Bof Bufon, C. C.; Deneke, C.; Schmidt, O. G. Nanomembrane-Based Mesoscopic Superconducting Hybrid Junctions. *Nano Lett.* **2010**, *10*, 3704–3709.